Three-Dimensional Gradient-Index Materials and Their Applications in Microwave Lens Antennas

Hui Feng Ma, Ben Geng Cai, Teng Xiang Zhang, Yan Yang, Wei Xiang Jiang, and Tie Jun Cui, *Senior Member, IEEE*

***Abstract*—In this paper, we introduce a method to realize 3-D inhomogeneous and nearly isotropic gradient-index materials in the microwave regime. The unit cells of such gradient-index materials are drilled-hole dielectric structures, which can be easily fabricated by using the traditional printed circuit boards. To demonstrate the feasibility of the proposed method, we design and realize two functional devices in the microwave frequencies—a half-spherical Luneburg lens and a half Maxwell fisheye lens—based on 3-D gradient-index materials. The measurement results show that both devices have very good performance, which have good agreements to the numerical simulations, illustrating the great application potentials of the 3-D gradient-index materials.**

***Index Terms*—Gradient-index materials, Luneburg lens, Maxwell fisheye lens, three dimensions.**

I. Introduction

GRADIENT-INDEX materials have the property that the index of refraction changes gradually according to the geometry. There have been several well-known functional devices based on gradient-index materials, such as Luneburg lens [1], Maxwell fisheye lens [2], Eaton lens [3], and Fresnel lens [4], which are very useful in the engineering applications. Hence, how to fabricate such gradient-index materials is a key point to realize the above functional devices. Take the Luneburg lens and the Maxwell fisheye lens as examples. The Luneburg lens has a gradient distribution of the index of refraction in a sphere: $n = (2 - r^2/R^2)^{1/2}$, where R is the sphere radius. The Luneburg lens can guide the incoming collimated rays from infinity to a focal point on the opposite surface of the lens [1]; hence, it can be used as a good antenna in the microwave regime. The Maxwell fisheye lens, which was proposed in 1854 with the distribution of index of refraction as $n = n_0/(1 + r^2/R^2)$ [2], is a type of imaging device to transform a point source at the lens surface into a focus at the diametrically opposite side of the lens. Half-spherical Luneburg lens and half fisheye lens have also important applications as high-directive microwave antennas [5]–[8]. Traditionally, the Luneburg and fisheye lenses have been produced by a series of concentric inhomogeneous dielectric shells, whose electric permittivity is varied discretely from 1 to 4 [5]–[10]. However, the fabrication of such concentric dielectric shells is quite complicated and there exists impedance mismatch among dielectric shells, which will degrade the performance. There have been some interesting works for designing the Luneburg lenses by using artificial electromagnetic structures [11]–[14]: the refractive index of the lens is controlled by drilled holes and changing the geometry dimension of dielectrics [11], [12], or by designing special metal surface structures on printed circuit boards (PCBs) to realize the desired index [13], [14]. However, such Luneburg lenses are planar structures, in other words, they are all 2-D cases.

Based on the effective medium theory [15], gradient-index materials can be designed by cell to cell using a series of electromagnetic unit cells, whose dimension is about one-tenth wavelength. Because the unit cells are small enough, the structures composed of such unit cells can be treated as an effective medium accurately. Each unit cell can be designed independently to achieve the desired index of refraction. Hence, the gradient-index materials can be fabricated accurately and nearly continuously. Meanwhile, because of cell-to-cell design, the change in impedance for adjacent cells is minor, resulting in good impedance match. A 3-D flattened Luneburg lens based on transformation optics has been developed [16] in our previous work.

In this paper, we propose a general method to realize 3-D inhomogeneous and nearly isotropic gradient-index materials using the drilled-hole approach on the commercial dielectric boards. Based on the proposed method, we have designed and fabricated two 3-D microwave gradient-index materials devices: a half-spherical Luneburg lens and an impedance-matched half-spherical Maxwell fisheye lens, which have excellent performance in radiating high-directivity beams in the designed directions and hence can be used as high-performance lens antennas.

Different from the traditional approach in the realization of the Luneburg and fisheye lenses, gradient-index materials can make the impedance change between two adjacent unit cells very small to generate high directivity with low return loss. Recently, there have been several papers on Luneburg lens and fisheye lens made of gradient-index materials [17]–[21] based on the effective medium, but all of them are 2-D mimicking. In this paper, 3-D half-spherical Luneburg and fisheye lenses are

Manuscript received July 07, 2012; revised September 29, 2012; accepted December 26, 2012. Date of publication January 03, 2013; date of current version May 01, 2013. This work was supported in part by the National Science Foundation of China under Grants 60990320, 60990321, 60990324, 61138001, 61171024, and 61171026, in part by the National High-Tech Project under Grants 2011AA010202 and 2012AA030402, and in part by the 111 Project under Grant 111-2-05.

The authors are with the State Key Laboratory of Millimeter Waves and the Institute of Target Characteristics and Identification, School of Information Science and Engineering, Southeast University, Nanjing 210096, China (e-mail: hfma@emfield.org; bgcai@emfield.org; txzhang_eric@utexas.edu; yyan1024@hotmail.com; wxjiang@emfield.org; tjcui@seu.edu.cn).

Color versions of one or more of the figures in this paper are available online at http://ieeexplore.ieee.org.

Digital Object Identifier 10.1109/TAP.2012.2237534

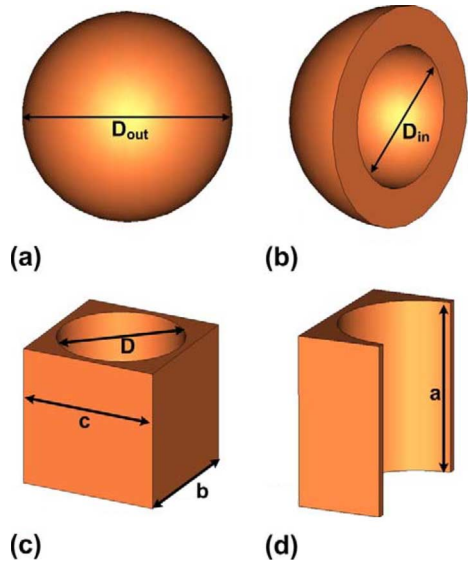

Fig. 1. 3-D gradient-index material unit cells. (a), (b) Spherical dielectric shell unit cell, whose outer diameter is Dout and inner diameter is Din. (c), (d) Drilled-hole dielectric cuboid unit cell, whose side lengths are a, b, and c with the diameter of via hole D.

produced by nearly isotropic gradient-index materials, which are realized using the commercial PCBs (F4B and FR4), with the relative permittivity 2.65 and 4.4 and loss tangent 0.001 and 0.025, respectively. Such gradient-index material lenses are designed, fabricated, and measured, which have good performance of high gain, narrow half-power beam width, and low loss over a broad bandwidth from 12 to 18 GHz (the Ku band).

II. Materials and Methods

In nature, most materials are made up of molecules and atoms, both of which have spherical symmetry, and hence are isotropic. Similarly, to realize 3-D isotropic gradient-index materials, which are made up of nonperiodic artificial structures, the unit cell should also have the spherical symmetry, as shown in Fig. 1(a) and (b). However, in the microwave frequency, it is difficult to fabricate 3-D gradient-index materials by using the spherical unit cells. An easy way to realize nearly isotropic gradient-index materials is to use the drilled-hole dielectric unit cell, as demonstrated in Fig. 1(c) and (d). Such a unit cell can be treated as approximately isotropic and is easy to fabricate by using the PCB technology. Fig. 1(c) illustrates a whole unit cell, in which the side lengths and diameter of the via-hole are a, b, c, and D, respectively. The effective index of refraction of the unit cell can be controlled by changing the via-hole diameter, D. Fig. 1(d) shows the sectional drawing of the unit cell.

To investigate the characteristics of the drilled-hole 3-D gradient-index materials based on PCBs (FR4 and F4B), we make a detailed analysis. From the effective medium theory [12], the effective indices of refraction are obtained, and their variations to the PCB dielectrics, unit heights, and via-hole diameters are demonstrated in Fig. 2. Here, P1, P2, and P3 represent different polarizations for the electrical field parallel to length a, length b, and length c, separately, as shown in Fig. 2(a). In our design, a, b, and c are all set as 2 mm (0.1 wavelength at 15 GHz) to obtain the required indices of refraction. Hence, the unit cells

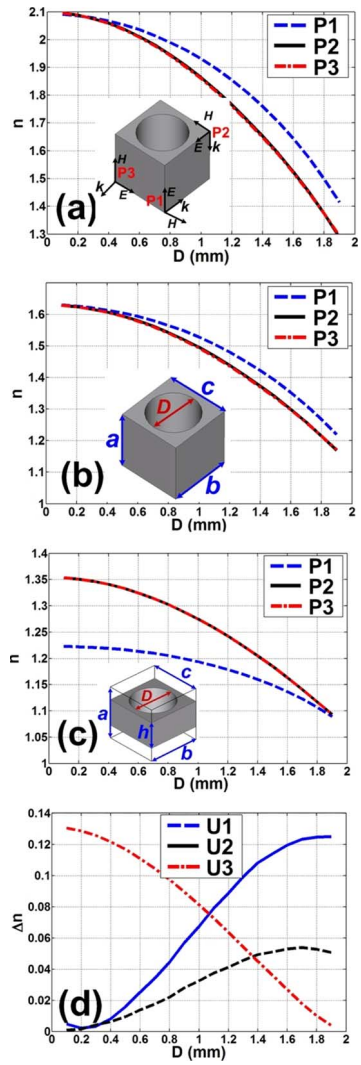

Fig. 2. Effective medium parameters under different polarizations. (a) $2 \times 2 \times 2$mm^3 FR4 dielectric unit cell (U1). (b) $2 \times 2 \times 2$ mm^3 F4B dielectric unit cell (U2). (c) $2 \times 2 \times 1$ mm^3 F4B dielectric unit cell (U3). (d) The errors between P1 and P2 (or P3) as the via-hole diameter changes gradually.

investigated in this paper are used in the Ku band (12–18 GHz), whose central frequency is 15 GHz. Similarly, the unit cells can also be designed in other frequency bands using different dimensions [21].

Fig. 2(a) and (b) illustrates the indices of refraction for the $2 \times 2 \times 2$ mm3 FR4 (U1) and F4B (U2) unit cells with different via-hole diameters, from which we notice that the refractive index (n) decreases gradually as the diameter (D) increases. The above results also show that the unit cells have the same responses for the P2 and P3 polarizations, as depicted in the black solid line and red dashed line in Fig. 2(a) and (b). The response for the P1 polarization has a small difference from those for the P2 and P3 polarizations, as shown in the blue dashed line. When D increases, the index for P1 polarization becomes larger compared to the P2 and P3 polarizations.

Fig. 2(c) demonstrates the effective refractive index of the $2 \times 2 \times 1$ mm3 F4B (U3) unit cell, whose height is 1 mm. Unlike the cases of U1 and U2 cells, the refractive index of U3

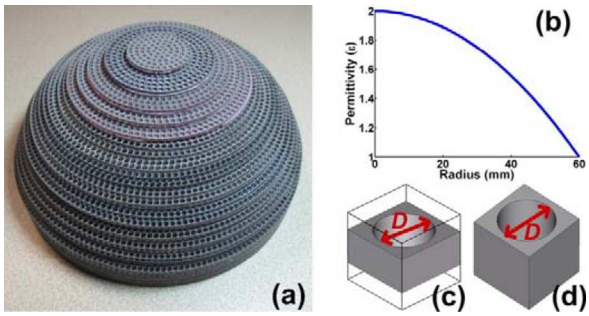

Fig. 3. Fabrication of the half spherical Luneburg lens. (a) The photograph of the lens. (b) The permittivity of the Luneburg lens varying along the radius. (c) $2 \times 2 \times 1\text{mm}^3$ F4B unit cell. (d) $2 \times 2 \times 2\ \text{mm}^3$ F4B unit cell.

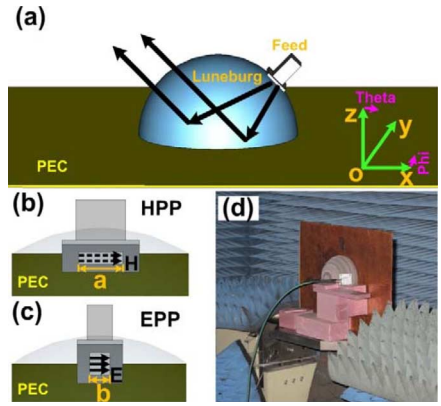

Fig. 4. Measurement demonstration of the half spherical Luneburg lens, in which the lens radius is 70 mm, and side lengths of feed are $a = 16$ mm and $b = 8$ mm, respectively. (a) A half spherical Luneburg lens combined with a PEC plate. (b) The HPP polarization, in which the long side of feed is parallel to the PEC plate. (c) The EPP polarization, in which the short side of feed is parallel to the PEC plate. (d) The measurement setup in a fully anechoic microwave chamber.

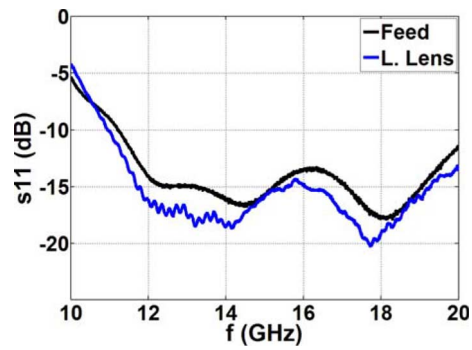

Fig. 5. Measured return loss of the feeding source and half-spherical Luneburg lens antenna, in which black solid line is the S11 of feeding source and blue solid line is the S11 of the half-spherical Luneburg Lens.

for the P1 polarization becomes smaller compared to the P2 and P3 polarizations as D increases. The solid blue line and black dashed line in Fig. 2(d) give the errors of n between P1 and P2/P3 polarizations for U1 and U2 cells, respectively. We observe that, as D increases from 0.1 to 1.9 mm, the error of n is varied from 0 to 0.125 for U1, while varied from 0 to 0.55 for U2. Differently, the error of n is decreased from 0.13 to 0 for U3, as D increases from 0.1 to 1.9 mm. In order to design the nearly isotropic 3-D gradient-index materials, we chose U1 to realize the refractive indices between 2.1 and 1.63 by changing D from 0.1 to 1.4 mm; chose U2 to realize indices between 1.63 and 1.18 by changing D from 0.1 to 1.9 mm; and chose U3 to realize indices between 1.18 and 1.1 by changing D from 1.5 to 1.9 mm. Using the above three kinds of unit cells, we can design arbitrarily 3-D nearly isotropic and inhomogeneous metamaterials with the refractive index changing from 2.1 to 1.

III. Two Kinds of Gradient-Index Material Lens

Using the proposed inhomogeneous and nearly isotropic 3-D gradient-index materials, we have designed, fabricated, and measured two functional devices: half-spherical Luneburg lens antenna and half-spherical fisheye lens antenna. Measurement results show very good performance of such devices.

A. The 3-D Half-Spherical Luneburg Lens

The designed half-spherical Luneburg lens is given in Fig. 3(a). According to the distribution of refractive index, the permittivity of Luneburg lens varies from 2 to 1 continuously from the spherical centre to surface, as illustrated in Fig. 3(b). Hence, we only need the $2 \times 2 \times 1\ \text{mm}^3$ and $2 \times 2 \times 2\ \text{mm}^3$ F4B unit cells depicted in Fig. 3(c) and (d) to realize the corresponding index of refraction.

In our experiments, we begin to design the Luneburg lens with radius of $R = 70$ mm, and the final fabricated lens has the radius of $R' = 65$ mm. A Ku-band (12.3–18 GHz) coax-to-waveguide transition with aperture size of $16 \times 8\ \text{mm}^2$ is used as the feeding source, and a PEC plate is attached to the half Luneburg lens as the reflector, as demonstrated in Fig. 4(a). Two polarizations have been considered in our measurements by adjusting the polarizations of feeding device: perpendicular polarization, in which the magnetic field is parallel to the PEC plate (HPP), as shown in Fig. 4(b), and parallel polarization, in which the electric field is parallel to the PEC plate (EPP), as shown in Fig. 4(c). Far fields of the Luneburg lens antenna were measured in a fully anechoic microwave chamber, and Fig. 4(d) illustrates the experiment setup of the measurement.

The return loss was measured using the Agilent Vector Network Analyzer N5230c (10 MHz–40 GHz), as shown in Fig. 5. The results show that the return loss of feeding source (black solid line in Fig. 5) and the half-spherical Luneburg lens antenna (blue solid line in Fig. 5) are lower than -13.7 dB and -14.2 dB in a wide frequency range from 11.6 to 19.4 GHz, respectively, implying that the antenna has low reflection over the whole Ku band.

In the measurements of far-field features, we first consider the HPP polarization, in which the long side b of the feeding device is parallel to the PEC plate and hence the magnetic field emitting from the feed is also parallel to the PEC plate, as shown in Fig. 4(b). The measured far-field radiation patterns under the HPP polarization are illustrated in Fig. 6. Here, Fig. 6(a) shows the E-plane patterns at 12.5, 15, and 18 GHz, respectively, in which the measurement plane is parallel to the XOZ plane (i.e., $\varphi = 0$). Because the feeding device is placed at $R = 70$ mm with $\varphi = 0$ and $\theta = 45°$, the waves will be transformed into plane waves, and emitted from the direction $\varphi = 0$ and $\theta = -45°$ by propagating through the half Luneburg lens and be reflected by the PEC plate. The radiation patterns on the

E plane demonstrate that the half-power bandwidths (HPBWs) are narrow, and the sidelobes are lower than -10 dB within the whole Ku band. Fig. 6(b) depicts the H-plane far-field radiation patterns at 12.5, 15and 18 GHz, respectively, in which the measurement plane is parallel to the plane with $\theta = -45^\circ$. The H-plane patterns also show the narrow HPBWs and low sidelobes (less than -20 dB in the whole Ku band).

In measurements of the EPP polarization, the short side a of the feeding device is parallel to the PEC plate, so that the electric field emitting from the feed is parallel to the PEC plane, as shown in Fig. 4(c). Similar to HPP polarization, we also measure both E- and H-plane radiation patterns under the EPP polarization, as depicted in Fig. 6(c) and (d), respectively. We observe that the sidelobes in E and and H planes are lower than -10 dB and -17 dB in the whole Ku band. The measured sidelobes, gains and efficiencies of the half-spherical Luneburg lens antennas under HPP and EPP polarizations are shown in Table I. The results show that the sidelobes in E and H planes for both HPP and EPP polarizations are smaller than -9 dB and -15 dB in the whole Ku band, respectively. The gains range from 23 to 24.5 dB under the EPP polarization, and range from 24.4 to 25.7 dB under the HPP polarization, over the whole Ku band. In order to further investigate the performance of the designed half-spherical Luneburg antenna, we calculate the efficiency of the antenna under both EPP and HPP polarizations. The efficiency is defined as $\varepsilon_{\text{ant}} = G_m/D_{\max}$, in which G_m is the measured gain, and $D_{\max}$ is maximum directivity corresponding to the uniform aperture illumination, which is defined as

$$D_{\max} = \frac{4\pi A_p}{\lambda^2} \tag{1}$$

where $A_p = \pi R^2$ is the physical aperture of the lens, and λ is the wavelength. The measured efficiencies are illustrated in Table I, which show that the efficiencies under the HPP polarization are larger than that of the EPP polarization.

The unit cells to realize the lens are almost isotropic, but they still have minor anisotropy according to Fig. 2. Hence, in order to show the sensitivity to fabrication tolerance of the designed half-spherical Luneburg lens, we carry out a full wave simulation of the same lens with ideal isotropy using commercial software, CST-Microwave studio. In simulation, the radius of Luneburg is $R_s = 70$ mm, whose index of refraction is isotropic and obeys $n_s = (2-r^2/R_s^2)^{1/2}$. The lens is discretized by using 35 spherical shells with different indexes, and the thickness of each shell is 2 mm.

Because of the length limitation, only the HPP polarization is considered for comparison. Fig. 7 shows far-field radiation patterns of the simulation and measurement results at 15 GHz. Except that the measured sidelobe on the E plane in the direction of -50 degrees is 8 dB higher than the simulation, the two results have good agreements with each other.

Fig. 8(a) and (b) gives the simulated and measured sidelobes on E and H planes, respectively. The biggest error between simulated and measured sidelobes on the E plane is at 15 GHz, where the measurement is about 7 dB higher than the simulation; while the biggest error on the H plane is at 14 GHz, where the measurement is about 10 dB higher than simulation.

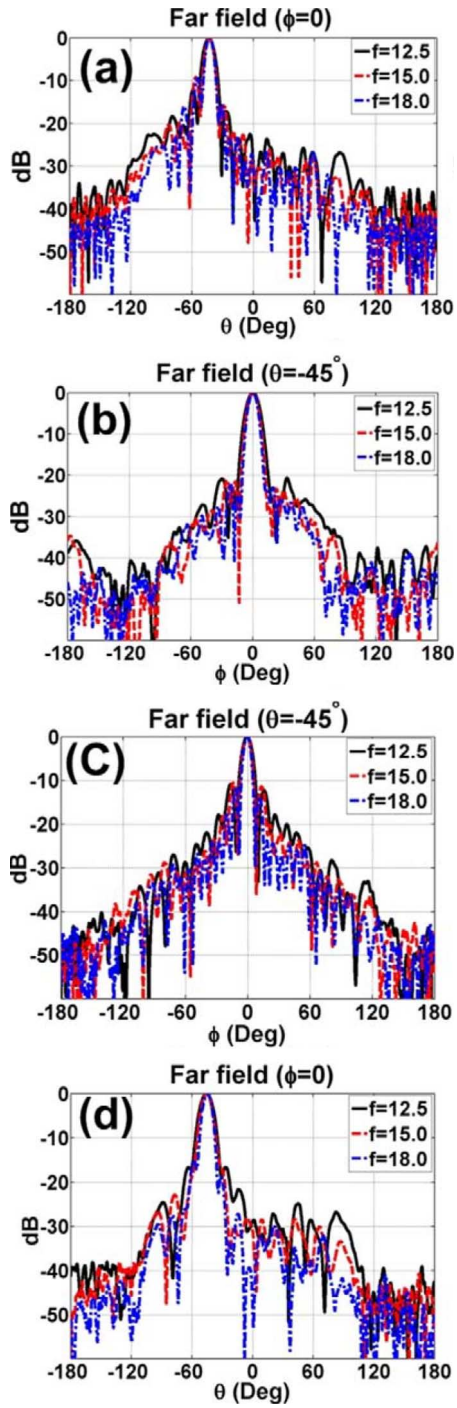

Fig. 6. Measured far-field radiation patterns of the half Luneburg lens antenna. (a), (b) The HPP polarization, in which the main lobes direct to $\varnothing = 0$ and $\theta = -45^\circ$; (a) indicates the E-plane patterns measured on the plane $\theta = -45^\circ$; while (b) indicates the H-plane patterns measured on the plane $\varnothing = 0$. (c), (d) The EPP polarization, in which the main lobes direct to $\varnothing = 0$ and $\theta = -45^\circ$; (c) indicates the E-plane patterns measured on the plane $\varnothing = 0$; while (d) indicates the H-plane patterns measured on the plane $\theta = -45^\circ$.

The simulated directivities and measured gains are shown in Fig. 8(c), and the biggest error happens at 18 GHz, where the simulated directivity is 1.8 dB higher than the measured gain. The above results show that the sidelobes of measured results are higher than simulations at some frequencies. Except sidelobes, the measured and simulated results have good

TABLE I
THE FAR-FIELD CHARACTERISTICS OF MEASURED RESULTS FOR HALF-SPHERICAL LUNEBURG LENS ANTENNA

f/GHz	Sidelobe (dB)				Gain (dB)		Efficiency (%)	
	HPP		EPP		HPP	EPP	HPP	EPP
	E Plane	H plane	E plane	H plane				
13	-13.3	-19.9	-10.6	-20.8	24.3	23.1	85.9	65.2
14	-11.7	-17.2	-11.4	-20.8	25.3	23.7	93.3	65.3
15	-9.2	-21.1	-10.5	-22.8	25.3	23.3	81.3	51.3
16	-11.3	-18.9	-10.4	-25.0	25.7	24.1	78.3	54.2
17	-10.5	-18.4	-11.9	-16.8	25.7	24.4	69.4	51.4
18	-9.5	-22.1	-11.5	-15.1	25.3	24.5	56.4	46.9

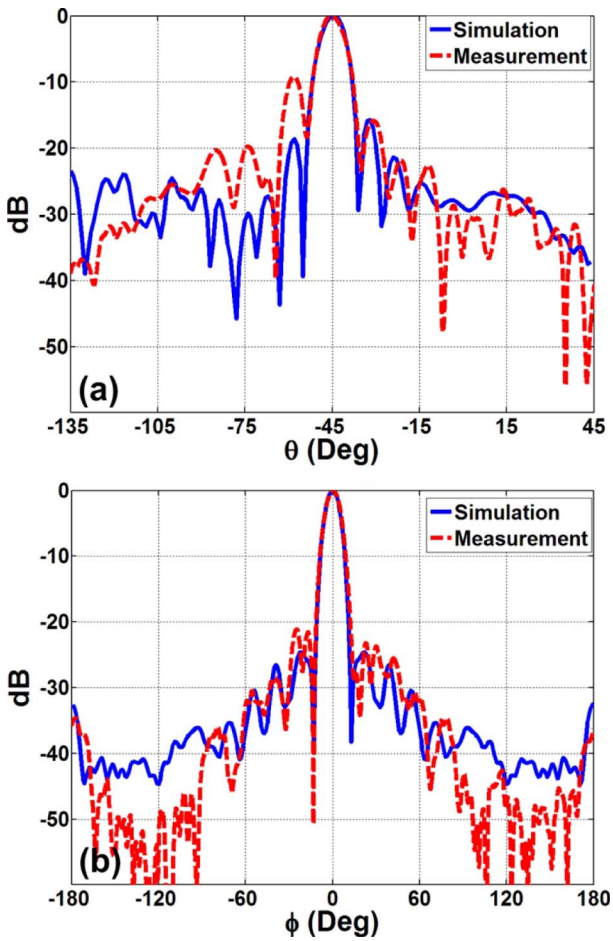

Fig. 7. Simulated and measured far-field radiation patterns of the half Luneburg lens antenna under the HPP polarization at 15 GHz. (a) The E-plane patterns simulated and measured on the plane of $\theta = -45^\circ$. (b) The H-plane patterns simulated and measured on the plane of $\varnothing = 0$.

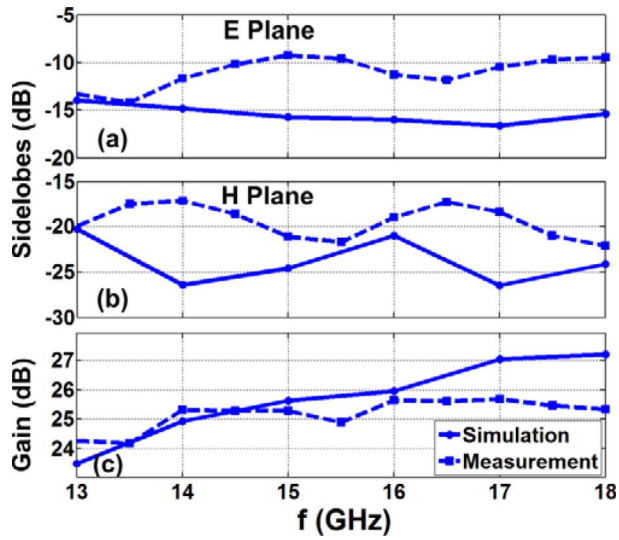

Fig. 8. Simulated and measured sidelobes and gains of the half-spherical Luneburg lens antenna over the whole Ku band, in which the solid and dashed lines represent simulated and measured results, respectively. (a) The sidelobes on E-plane. (b) The sidelobes on H-plane. (c) The gains.

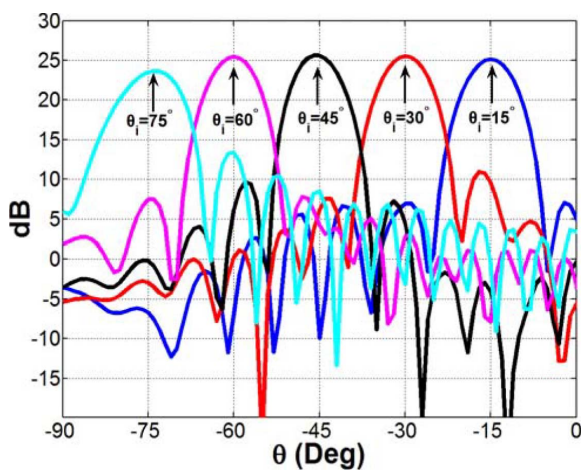

Fig. 9. Simulated far-field radiation patterns for different incident angles.

agreements, particularly for the far-field radiation patterns, as shown in Fig. 7. In Fig. 8, the measurement results show larger sidelobes and lower directivities than simulations, which may be caused by the following reason. In simulations, the half-spherical Luneburg lens is modeled by using CST with ideal lossless dielectrics. In experiments, however, the sample is fabricated by using PCBs (F4B), whose loss tangent is 0.001, and the PCB plates are bonded by using double-sided tapes. Since dozens of PCB plates are used to form the half-spherical Luneburg lens, the total error caused by double-sided tapes cannot be ignored. Hence, the losses of PCBs and double-sided tapes are possibly two key factors to lead to higher sidelobes and lower gains in experiments.

In order to show the advantage of Luneburg lens antenna, which can be worked for all incident angles, we carried out the full-wave simulations when the feeding source is located at different incident angles. In Fig. 9, the simulated far-field radiation patterns under HPP polarizations show that the main lobes of the half-spherical Luneburg lens antenna appear in the directions $\theta = -15^\circ, -30^\circ, -45^\circ, -60^\circ$, and -75° when the incident angle is $\theta = 15^\circ, 30^\circ, 45^\circ, 60^\circ$, and 75°, respectively,

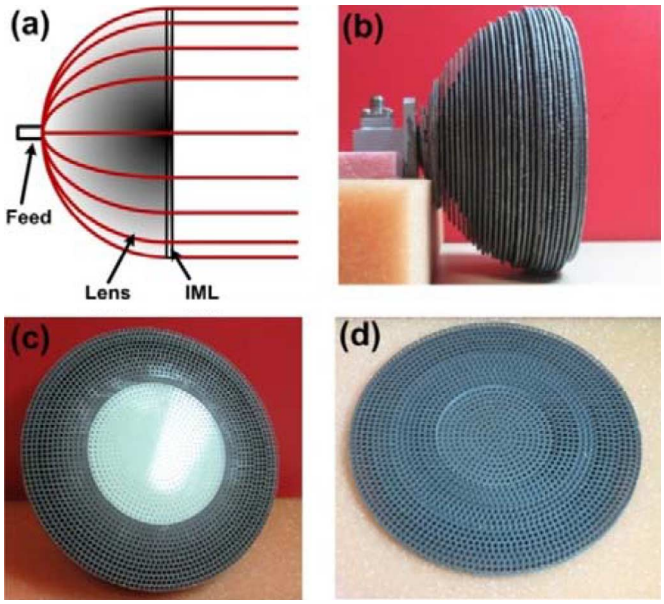

Fig. 10. Sketch and fabrication of the half-spherical fisheye lens. (a) Sketch of lens. (b) Photograph of the fabricated lens. (c) Photograph of the fisheye lens body. (d) Photograph of IML.

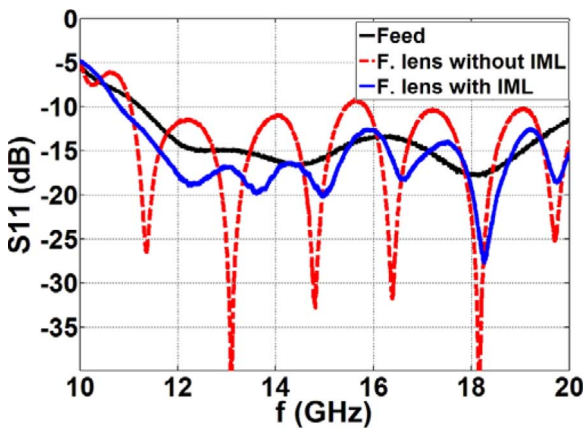

Fig. 11. Measured return loss of the feeding source (black solid line), the half-spherical fisheye lens antenna without (blue solid line) and with (red dashed) impedance matching layer.

in which $\varphi = 0$. The above results show that the half-spherical Luneburg lens can be operated for different incident angles with good performance.

B. The 3-D Half-Spherical Fisheye Lens

The other device we have designed is a 3-D half-spherical fisheye lens, whose index distribution is $n = 2(1+r^2/R^2)-1$, where R is the radius of the lens, and $0 < r < R$. A sketch of the designed lens is shown in Fig. 10(a), which includes three parts: the feeding source, lens, and the impedance matching layer (IML). Here, IML is designed using a single-layer quarter-wave transformer to reduce the reflection on the air-lens interface. The demonstration shows that the quasi-spherical waves emitted from the feed source are transformed to plane waves after propagating through the half lens, as illustrated in Fig. 10(a). Using the proposed 3-D nearly isotropic gradient-index materials, we design the half-spherical fisheye lens

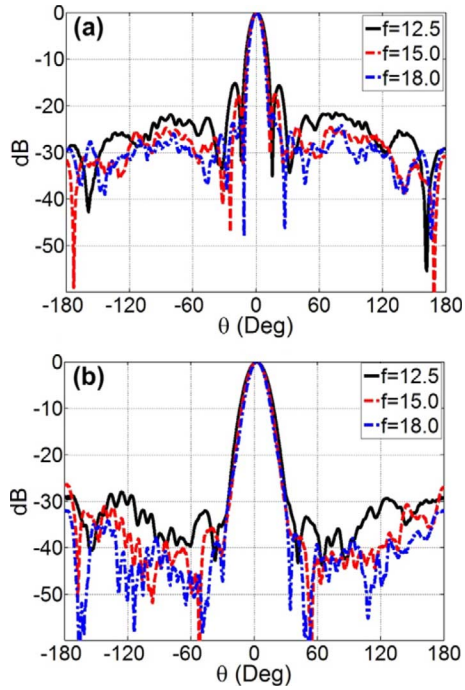

Fig. 12. Measured far-field radiation patterns of the half-spherical fisheye lens antenna. (a) E-plane. (b) H-plane.

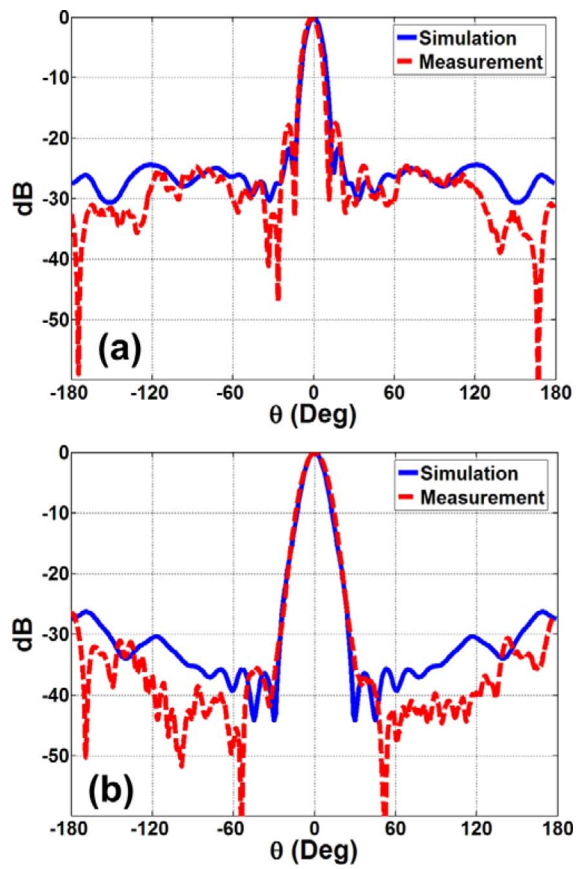

Fig. 13. Simulated and measured far-field radiation patterns of the half f lens antenna under HPP polarization at 15 GHz. (a) E-plane. (b) H-plane.

with the radius $R = 60$ mm, and the final fabricated lens has the radius of $R' = 55$ mm. Fig. 10(b) is the photo picture of

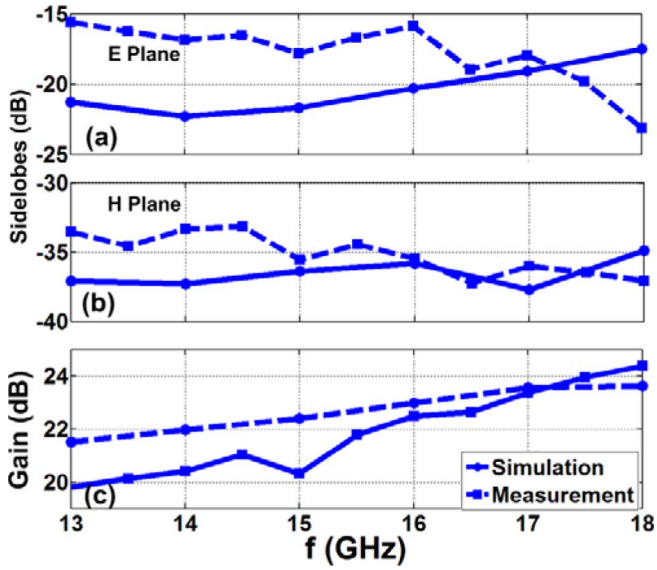

Fig. 14. Simulated and measured sidelobes and gains of the half-spherical fisheye lens antenna over the whole Ku band, in which the solid and dashed lines represent simulated and measured results, respectively. (a) The sidelobes on E-plane. (b) The sidelobes on H-plane. (c) The gains.

TABLE II
FAR-FIELD CHARACTERISTICS OF MEASURED RESULTS FOR THE HALF-SPHERICAL FISHEYE LENS ANTENNA

f/GHz	Sidelobe (dB)		Gain (dB)	Efficiency (%)
	E plane	H plane		
13	-15.6	-33.6	19.8	42.6
14	-16.9	-33.3	20.4	42.2
15	-17.8	-35.6	20.3	36.7
16	-15.9	-35.5	22.5	52.4
17	-18.0	-36	23.3	55.6
18	-23.2	-37.1	24.3	62.6

the fabricated lens system, including the feeding source and IML. The feeding source used here is the same as that in the Luneburg lens. The detailed fisheye lens and IML are given in Fig. 10(c) and (d). For the fisheye lens body, all three kinds of unit cells U1, U2, and U3 are required to realize the indices of refraction from 1 to 2; and for IML, whose index obeys the rule of $n_{\mathrm{IML}} = n_1/2$, only the unit cells U2 and U3 are needed to realize the index from 1 to 1.414.

Fig. 11 demonstrates the measured return losses of the fabricated lens from the Agilent Vector Network Analyzer N5230c, in which the blue solid line and red dashed line represent the cases with and without IML, respectively. The results show that the reflection from the air-lens interface is significantly decreased after using IML, which is lower than -12 dB in the wide frequency band from 11.5 to 20 GHz, as seen in Fig. 11. The far-field radiation patterns of the fisheye lens on the E and H planes are illustrated in Fig. 12, from which we notice that the sidelobes in E- and H-plane patterns are lower than -15 dB and -30 dB over the whole Ku band, respectively. The back scattering in the H plane is a little bit higher, but it is still smaller than -27 dB.

Similar to the half-spherical Luneburg lens, we also calculate the efficiency of the half-spherical fisheye lens, as illustrated in Table II. Meanwhile, in order to investigate the sensitivity of

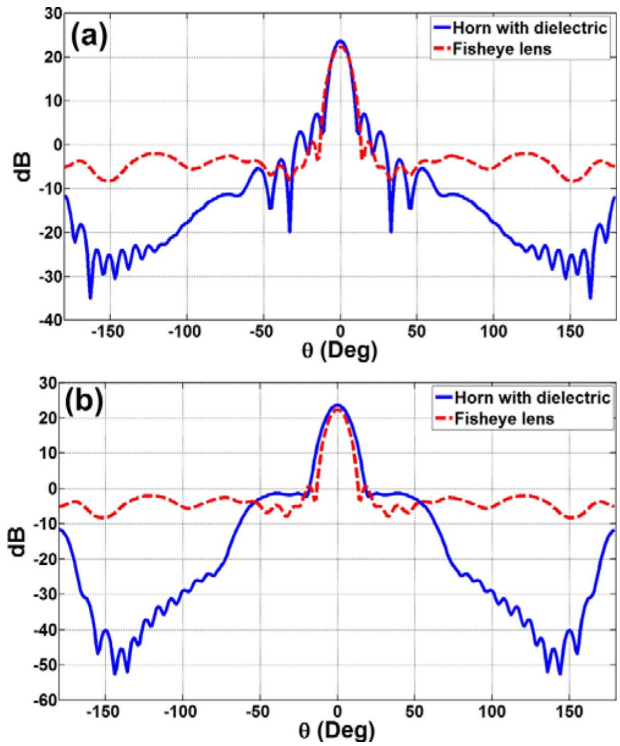

Fig. 15. Simulated far-field radiation patterns of the horn antenna with dielectric lens and half-spherical fisheye lens antenna. (a) The E plane. (b) The H plane.

fabrication tolerance and experimental errors of the designed lens, we make the corresponding full-wave simulations using CST. In our simulation, the radius of half-spherical fisheye lens is $R_s = 60$ mm, whose index of refraction is isotropic and obeys $n = n_0/(1 + r^2/\mathrm{Rs}^2)$. The lens is discretized by 30 spherical shells with different index in the simulation model, and the thickness of each shell is 2 mm. The simulated and measured far-field radiation patterns have good agreements at 15 GHz, as shown in Fig. 13. Fig. 14(a) and (b) is simulated and measured sidelobes on E and H planes, respectively. The measurements are generally higher than the simulations, but the error is smaller when the frequency is higher. Fig. 14(c) gives the simulated directivities and measured gains of the half-spherical fisheye lens. Similar to the case of half-spherical Luneburg lens antenna, the measurement results have higher sidelobes and lower gains than simulations due to the same reason. However, compared to the half Luneburg lens, the fisheye lens shows better agreements between simulations and measurements.

To further investigate the performance of the half-spherical fisheye lens, a horn antenna with dielectric [22] with aperture diameter $D_2 = 60$ mm was simulated to compare with the fisheye lens at 15 GHz. The dielectric inserted in horn is a hyperbolic lens with permittivity $\varepsilon_r = 2$, which is generated from the equation $z^2/u^2 - (x^2 + y2)/v^2 = 1$, where $u = 30$ mm and $v = 52$ mm. According to the simulation results as shown in Fig. 15, the directivity of the horn antenna with dielectric (23.6 dB) is 1.2 dB higher than that of the fisheye lens (22.4 dB), but the side lobes of the horn antenna with dielectric (-16.3 dB and -25 dB for E- and H planes) are higher than those of fisheye lens (-21.7 dB and -36.4 dB for E- and H planes), and the

half-power bandwidths of two antennas are the same for both E plane (11°) and H plane (14°). The far-field radiation patterns of two antennas show that the back scattering of the horn antenna with dielectric is smaller than that of the half-spherical fisheye lens.

IV. Conclusion

In this paper, an easy method for designing and fabricating 3-D inhomogeneous and nearly isotropic gradient-index materials has been presented, from which two 3-D gradient-index material devices, half-spherical Luneburg and fisheye lenses, have been realized in the Ku band. The losses in the designed 3-D gradient-index materials are small enough since the unit cells are nonresonant structures, in which the imaginary part of the effective index of refraction is nearly zero. The measurement results illustrated very good performance of two lenses, which also have good agreements with the isotropic simulation results. This paper provides a way to realize general 3-D inhomogeneous and nearly isotropic gradient-index material devices.

References

[1] R. K. Luneberg, *Mathematical Theory of Optics*. Providence, RI, USA: Brown Univ. Press, 1944.

[2] J. C. Maxwell, *Cambridge Dublin Math. J.*, vol. 8, pp. 188–188, 1854.

[3] J. E. Eaton, An Extension of the Luneburg Type Lenses Naval Res. Lab., 1953, Res. Rep., no. 4110.

[4] A. Petosa and A. Ittipiboon, "Design and performance of a perforated dielectric Fresnel lens," *IEE Proc. Microw., Antennas, Propag.*, vol. 150, no. 5, pp. 309–314, Oct. 2003.

[5] B. Fuchs, L. L. Coq, O. Lafond, S. Rondineau, and M. Himdi, "Design optimization of multishell Luneburg lenses," *IEEE Trans. Antennas Propag.*, vol. 55, no. 2, pp. 283–289, Feb. 2007.

[6] S. Rondineau, M. Himdi, and J. Sorieux, "A sliced spherical Lüneburg lens," *IEEE Antennas Wireless Propag. Lett.*, vol. 2, pp. 163–166, 2003.

[7] B. Fuchs, O. Lafond, S. Rondineau, and M. Himdi, "Design and characterization of half Maxwell fish-eye lens antennas in millimeter waves," *IEEE Trans. Microw. Theory Tech.*, vol. 54, no. 6, pp. 2292–2300, Sep. 2006.

[8] B. Fuchs *et al.*, "Comparative design and analysis of Luneburg and half Maxwell fish-eye lens antennas," *IEEE Trans. Antennas Propag.*, vol. 56, no. 9, pp. 3058–3062, Sep. 2008.

[9] K. A. Zimmerman and L. Runyon, "Luneburg lens and method of constructing sample," U.S. patent 5,677,796, Oct. 1997.

[10] P. C. Strickland, "Method for fabricating Luneburg lenses," U.S. patent 6,721,103 B1, Apr. 2004.

[11] K. Sato and H. Ujiie, "A plate Luneberg lens with the permittivity distribution controlled by hole density," *Electro. Commun. Jpn.*, vol. 85, no. 9, pt. 1, pp. 1–12, May 2002.

[12] X. Wu and J. J. Laurin, "Fan-beam millimeter-wave antenna design based on the cylindrical Luneburg lens," *IEEE Trans. Antennas Propag.*, vol. 55, no. 8, pp. 2147–2156, Aug. 2007.

[13] C. Pfeiffer and A. Grbic, "A printed, broadband Luneburg lens antenna," *IEEE Trans. Antennas Propag.*, vol. 58, no. 9, pp. 3055–3059, Sep. 2010.

[14] L. Xue and V. F. Fusco, "Printed holey plate Luneburg lens," *Microw. Opt. Technol. Lett.*, vol. 50, no. 2, pp. 378–380, Jun. 2007.

[15] R. Liu, T. J. Cui, D. Huang, B. Zhao, and D. R. Smith, "Description and explanation of electromagnetic behaviors in artificial metamaterials based on effective medium theory," *Phys. Rev. E*, vol. 76, p. 026606, Aug. 2007.

[16] H. F. Ma and T. J. Cui, "Three-dimensional broadband and broad-angle transformation-optics lens," *Nat. Commun.*, vol. 1, no. 24, pp. 1–7, 2010.

[17] H. F. Ma, X. Chen, X. M. Yang, H. S. Xu, Q. Cheng, and T. J. Cui, "A broadband metamaterial cylindrical lens antenna," *Chinese Sci. Bull.*, vol. 55, no. 19, pp. 2066–2070, Jul. 2010.

[18] Q. Cheng, H. F. Ma, and T. J. Cui, "Broadband planar Luneburg lens based on complementary metamaterials," *Appl. Phys. Lett.*, vol. 95, p. 181901, Nov. 2009.

[19] N. Kundtz and D. R. Smith, "Extreme-angle broadband metamaterial lens," *Nature Mater.*, pp. 129–132, 2010.

[20] A. D. Falco, S. C. Kehr, and U. Leonhardt, "Luneburg lens in silicon photonics," *Opt. Express*, vol. 19, pp. 5156–5162, 2011.

[21] Z. L. Mei, J. Bai, and T. J. Cui, "Experimental verification of a broadband planar focusing antenna based on transformation optics," *New J. Phys.*, vol. 13, pp. 1367–2630, 2011.

[22] D. K. John and R. J. Marhefka, *Antennas: For All Applications*, 3rd ed. New York, NY, USA: McGraw-Hill, 2002.

Hui Feng Ma was born in December, 1981, in Jiangsu, China. He received the B.Sc. degree in electronic engineering from the Nanjing University of Science and Technology, Nanjing, China, in 2004, and the Ph.D. degree from the State Key Laboratory of Millimeter Waves, Southeast University, Nanjing, in 2010.

He joined the School of Information Science and Engineering, Southeast University, September 2010 and was promoted to an Associate Professor in September 2011. He has published his first author journal papers in *Nature Communications*, *Applied Physic Letters*, *Optics Express*, etc. His current research interests involve metamaterial antennas, invisible cloaks, and other novel metamaterial functional devices including theoretical design and experimental realization.

In 2010, his research of three-dimensional ground carpet cloak realized by using of metamaterials have been selected as one of the "10 Breakthroughs of Chinese Science in 2010."

Ben Geng Cai was born in Zhejiang, China. He received the B.S. degree and the M.S. degree in physics from Zhejiang University, Hangzhou, China, in 2002 and 2005, respectively. He is currently working toward the Ph.D. degree in radio engineering from Southeast University, Nanjing, China.

His current research interests include in application of metamaterials in antenna, optical transformation and surface plasmons.

Teng Xiang Zhang received the B.Sc. degree in electrical engineer from Chien-Shiung Wu Honored College, Southeast University, Nanjing, China, in 2011. He is currently working toward the M.Sc. degree in electromagnetics and acoustic tracks at the University of Texas, Austin, TX, USA.

In 2009, he joined the State Key Laboratory of Millimeter Waves and worked on metamaterials and their applications on antennas. In September 2011, he joined the Metamaterials and Plasmonics Research Laboratory and worked on 2-D Luneburg lenses. He is currently a Graduate Research Assistant in the Wireless Networking Communications Group working on laptop antenna optimization.

Yan Yang received the M.S. degree from Chang'an University, Xi'an, China, in 2005, and the Ph.D. degree from the University of Southampton, Southampton, U.K., in 2011.

She joined the School of Information Engineering, Chang'an University, in 1999, and became a Lecturer in 2008. She is now working in the School of Information Science and Engineering, Southeast University, Nanjing, China, as an Associate Professor. Her research interests include the transportation engineering, human factor, in-vehicle design, and wireless devices for in-vehicle systems. She is a Principal Investigator of a project funded by the National Science Foundation of China.

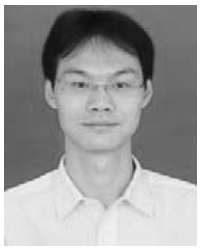

Wei Xiang Jiang was born in Jiangsu Province, China, in 1981. He received the B.S. degree in mathematics from Qingdao University, Qingdao, China, in June 2004 and the M.S. degree in applied mathematics in Mar. 2007 and Ph.D. degree in electrical engineering from Southeast University, Nanjing, China, in March 2007 and March 2011, respectively.

He was promoted to an Associate Professor in May 2011. His current research interests involve electromagnetic theory and metamaterials. His researches have been selected as Research Highlights in *Europhysics News Journal*, *Journal of Physics D*: *Applied Physics*, and *Applied Physics Letters*.

Dr. Jiang served as Organization Committee Co-Chair of the International Workshop on Metamaterials (META'2012).

Tie Jun Cui was born in Hebei, China, in September 1965. He received the B.Sc., M.Sc. and Ph.D. degrees in electrical engineering from Xidian University, Xi'an, China, in 1987, 1990, and 1993, respectively.

In March 1993, he joined the Department of Electromagnetic Engineering, Xidian University, and was promoted to an Associate Professor in November 1993. From 1995 to 1997 he was a Research Fellow with the Institut fur Hochstfrequenztechnik und Elektronik (IHE) at the University of Karlsruhe, Germany. In July 1997, he joined the Center for Computational Electromagnetics, Department of Electrical and Computer Engineering, University of Illinois at Urbana-Champaign, first as a Postdoctoral Research Associate and then a Research Scientist. In September 2001, he became a Cheung-Kong Professor with the Department of Radio Engineering, Southeast University, Nanjing, China. Currently, he is the Associate Dean with the School of Information Science and Engineering, and the Associate Director of the State Key Laboratory of Millimeter Waves. He is a coeditor of the book *Metamaterials—Theory, Design, and Applications* (Springer, 2009) and the author of six book chapters. He has published over 200 peer-review journal papers in *Science*, *PNAS*, *Nature Communications*, *Physical Review Letters*, IEEE Transactions, etc. His research interests include metamaterials, computational electromagnetic, wireless power transfer, and millimeter wave technologies.

Dr. Cui was awarded a Research Fellowship from the Alexander von Humboldt Foundation, Bonn, Germany, in 1995, received a Young Scientist Award from the International Union of Radio Science (URSI) in 1999, was awarded a Cheung Kong Professor under the Cheung Kong Scholar Program by the Ministry of Education, China, in 2001, received the National Science Foundation of China for Distinguished Young Scholars in 2002, received Special Government Allowance awarded by the Department of State, China, in 2008, received the Award of Science and Technology Progress from Shaanxi Province Government in 2009, was awarded by a May 1st Labour Medal by Jiangsu Province Government in 2010, and received the First Prize of Natural Science from Ministry of Education, China, in 2011. Dr. Cui's researches have been selected as one of the "10 Breakthroughs of Chinese Science in 2010," one of the "Best of 2010" in *New Journal of Physics*, *Research Highlights in Europhysics News Journal*, *Journal of Physics D: Applied Physics*, *Applied Physics Letters*, and *Nature China*. He is a member of URSI Commission B, and a Fellow of Electromagnetics Academy, MIT, USA. He was an Associate Editor for the IEEE TRANSACTIONS ON GEOSCIENCE AND REMOTE SENSING. He served as an Editorial Staff for the *IEEE Antennas and Propagation Magazine*, and is on the editorial boards of *Progress in Electromagnetic Research (PIER)* and *Journal of Electromagnetic Waves and Applications*. He served as General Co-Chair of the International Workshops on Metamaterials (META'2008, META'2012), the TPC Co-Chair of the Asian Pacific Microwave Conference (APMC'2005) and the Progress in Electromagnetic Research Symposium (PIERS'2004).